[21]M. Goldhaber and A. W. Sunyar, in *Alpha-, Beta-, and Gamma-Ray Spectroscopy*, edited by K. Siegbahn (North-Holland Publishing Company, Amsterdam, The Netherlands, 1965), Vol. 2, Chap. 18.
[22]L. S. Kisslinger and R. A. Sorensen, Kgl. Danske Videnskab. Selskab, Mat.-Fys. Medd. 32, No. 9 (1960).
[23]J. P. Unik, private communication.
[24]A. Lundan and A. Süvola, Ann. Acad. Sci. Fennicae A6, No. 288 (1968).
[25]N. R. Johnson and G. D. O'Kelley, Phys. Rev. 114, 279 (1959).
[26]P. A. Moore, P. J. Riley, C. M. Jones, M. D. Mancusi, and J. L. Foster, Jr., Phys. Rev. C 1, 1100 (1970).
[27]R. L. Watson, J. B. Wilhelmy, R. C. Jared, C. Rugge, H. R. Bowman, S. G. Thompson, and J. O. Rasmussen, Nucl. Phys. A141, 449 (1970).
[28]J. B. Wilhelmy, University of California Lawrence Radiation Laboratory Report No. UCRL-18979, 1969 (unpublished).
[29]T. Alvager, R. A. Naumann, R. F. Petry, G. Sidenius, and T. Darrah Thomas, Phys. Rev. 167, 1105 (1968).
[30]H. W. Schmitt, J. H. Neiler, and F. J. Walter, Phys. Rev. 141, 1146 (1966).

PHYSICAL REVIEW C VOLUME 2, NUMBER 4 OCTOBER 1970

Measurements of Static Quadrupole Moment of the First Excited 2^+ States of the Nuclei Pd^{106} and Pd^{110} by Heavy-Ion Coulomb Excitation*

R. Beyer,† R. P. Scharenberg, and J. Thomson
Department of Physics, Prudue University, Lafayette, Indiana 47907
(Received 27 April 1970)

The static quadrupole moments of the 511.7-keV 2^+ state in Pd^{106} and the 373.8-keV 2^+ state in Pd^{110} have been determined by employing Coulomb-excitation techniques. Foils ($\sim$175 $\mu g/cm^2$) of separated Pd isotopes were bombarded with 25- and 30-MeV O^{16} ions and 55- and 56-MeV S^{32} ions from the Purdue University and Argonne National Laboratory tandem accelerators. The angular distributions of the inelastically scattered ions were measured in coincidence with the deexcitation γ rays to determine the relative excitation probabilities. The experimental data were fitted using the Winther–de Boer multipole-Coulomb-excitation program so that the sign and magnitude of the static quadrupole moment could be extracted. The effect of higher excited states on the excitation probability of the 2^+ state has been calculated using the matrix elements determined by Robinson *et al.* and the Winther–de Boer program. Self-consistency of the oxygen and sulfur data suggests that the excitation via the second 2^+ state interferes constructively so as to increase the excitation probability. With this choice for the interference via the second 2^+ state, the values of the static quadrupole moments are $Q_{22}=-0.458\pm0.059$ b for Pd^{106} and $Q_{22}=-0.483\pm0.049$ b for Pd^{110}. If the excitation via the second 2^+ state interferes destructively, the values of the static quadrupole moments are $Q_{22}=-0.282\pm0.059$ b for Pd^{106} and $Q_{22}=-0.266\pm0.049$ b for Pd^{110}.

I. INTRODUCTION

The Pd isotopes are classic examples of vibrational nuclei. In Pd^{106} and Pd^{110}, both the one-phonon 2^+ state and the two-phonon 0^+, 2^+, 4^+ triplet states are present, as predicted by the pure vibrational model of the nucleus.[1,2] The Pd nuclei, therefore, can be considered good subjects on which to test predictions of the vibrational model of the nucleus. One prediction of this model is that the static electric quadrupole moment of the first quadrupole phonon (2^+) state should be zero. Recent experiments[3-10] have shown substantial static quadrupole moments for these states in vibrational nuclei.

Tamura and Udagawa[11] are able to account for substantial static quadrupole moments by considering the first and second excited 2^+ states to be composed of large admixtures of the one- and two-quadrupole phonon states in their anharmonic-vibrator model of the nucleus. The results of this experiment will be compared with the predictions of the anharmonic-vibrator and the pure rotational models of the nucleus.

The reorientation effect[12] can be the dominant interference effect in heavy-ion Coulomb excitation. The reorientation effect involves the interaction of the static electric quadrupole moment of the target nucleus in its excited state and the electric field gradient produced by the incident projectile. Since this electric field gradient can be computed, the value of the static quadrupole moment of the nucleus can be extracted by measuring the relative differential excitation cross

section as a function of projectile type and ion scattering angle. We have measured the static quadrupole moment of the first excited 2^+ state in Pd^{106} and Pd^{110} using the reorientation effect in Coulomb excitation.

II. THEORY

The advantage in using Coulomb excitation in nuclear studies is the electromagnetic interaction is well understood. It is important, therefore, that an appropriate physical separation be maintained between target and projectile ion. If such a separation is maintained, the electromagnetic transition between states in the target nucleus can be considered to be induced by the time-dependent electromagnetic field of a point charge in a classical hyperbolic orbit.[13] Under these conditions the differential inelastic cross section for excitation from an initial state i to a final state f is given by

$$\frac{d\sigma_{if}}{d\Omega}(\text{Inelastic}) = P_{if}(\xi, \theta_{\text{Ion}})\frac{d\sigma_R}{d\Omega}, \tag{1}$$

where $P_{if}(\xi, \theta_{\text{Ion}})$ is the excitation probability, ξ is the adiabaticity parameter, θ_{Ion} is the scattering ion, and $d\sigma_R/d\Omega$ is the Rutherford differential cross section. The excitation probability is given by

$$P_{if}(\xi, \theta_{\text{Ion}}) = (2I_i+1)\sum_{M_i M_f} |b_{if}|^2, \tag{2}$$

where b_{if} is the transition amplitude, M_i and M_f are the magnetic quantum numbers associated with states i and f, and I is the nuclear spin.

It is useful to expand the transition amplitudes by using second-order perturbation theory, because of the insight provided into the interaction:

$$b_{if}^{(2)} = b_{if}^{(1)} + \sum_n b_{inf}. \tag{3}$$

Here n represents an intermediate state, either a magnetic substate of the final state or another state. When the excitation probability is expanded to second order one may write

$$P_{if}^{(2)} = P_{if}^{(11)} + P_{if}^{(12)} + P_{if}^{(22)}. \tag{4}$$

$P_{if}^{(11)}$ is the first-order excitation probability, $P_{if}^{(12)}$ the interference between first and second order, and $P_{if}^{(22)}$ a second-order term which may be neglected in this approximation.

If the state n represents a magnetic substate of the final state, the deviation from first order can be written[14]

$$\frac{P_{if}^{(12)}}{P_{if}^{(11)}} = 1.32\frac{A_1}{Z_2}\frac{\Delta E}{1+A_1/A_2}Q_{22}K(\xi, \theta_{\text{Ion}}), \tag{5}$$

where A_1 represents the projectile atomic mass, A_2 the target atomic mass, Z_2 the target atomic number, $\Delta E = E_f - E_i$ the excitation energy, and $K(\theta_{\text{Ion}}, \xi)$ the orbital dependence, tabulated in Ref. 14. The reduced matrix element

$$M_{22} = \langle I_2 \| (i)^2 \mathfrak{M}(E2) \| I_2 \rangle$$

is related to the static electric quadrupole moment of the 2^+ state, Q_{22}, by

$$eQ_{22} = -\tfrac{4}{5}(\tfrac{2}{7}\pi)^{1/2}M_{22}. \tag{6}$$

A schematic energy level diagram for the first- and second-order excitation processes is shown in Fig. 1.

The influence that the static electric quadrupole moment of a state has on the excitation probability of that state is defined as the reorientation effect. From Eq. (5) it can be seen that a measurement of the excitation probability as a function of θ_{Ion} or A_1 can yield the value of Q_{22}. In Fig. 2 the deviation from first order of the excitation probability for 54-MeV sulfur ions and 25-MeV oxygen ions on Pd^{106} is shown for $Q_{22} = 1$ b. The effects are almost twice as large for sulfur as for oxygen, indicating one reason for using heavier-ion beams.

For small excitation probabilities the assumption that the intermediate state n is a magnetic of the final state is usually valid. For larger excitation probabilities it may be necessary to consider the nearby states in any calculation designed to extract Q_{22}.

III. EXPERIMENT

The relative excitation probability may be evaluated using the relation

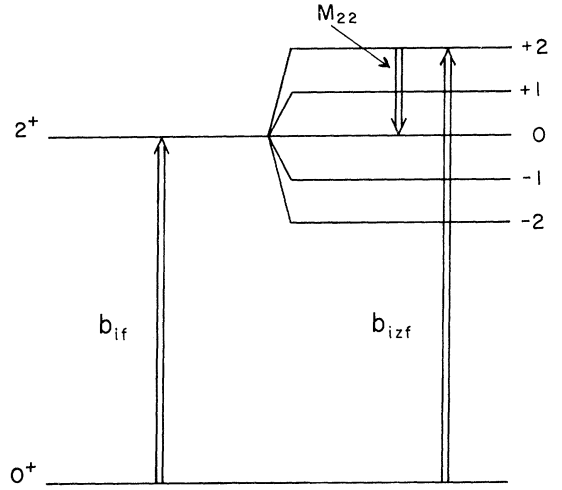

FIG. 1. Schematic energy-level diagram for first- and second-order processes in excitation of the first excited 2^+ state.

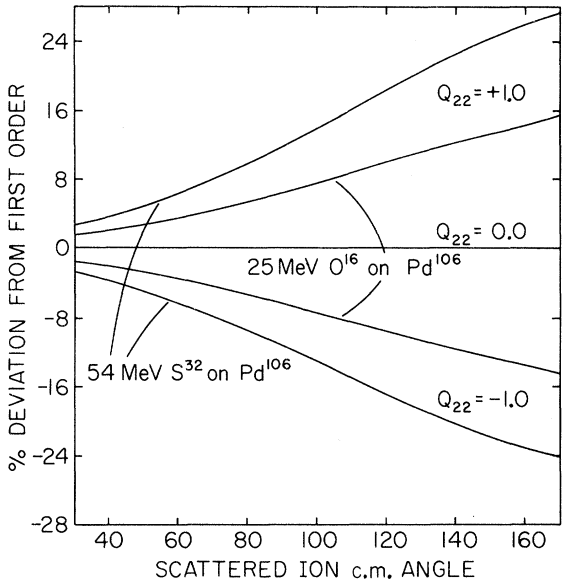

FIG. 2. Deviation from first-order excitation probability of first excited 2^+ state for 54-MeV S^{32} and 25-MeV O^{16} ions on Pd^{106} for $Q_{22}=\pm 1$ b.

$$P_{if}(\xi, \theta_{\text{Ion}}) = \frac{d\sigma_{if}}{d\Omega}(\text{Inelastic}) \Big/ \frac{d\sigma_R}{d\Omega}. \tag{7}$$

We have chosen to measure the relative excitation probability as a function of ion scattering angle and to identify the inelastic events by requiring a coincidence between a deexcitation γ photon and a scattered ion. The experimental arrangement is indicated in Fig. 3.

The deexcitation γ photons were detected in a 22.85-cm × 10.15-cm NaI(Tl) crystal positioned with the front face of the crystal 3.18 cm from the target. The crystal symmetry axis was placed directly above the target center and perpendicular to the scattering plane. The crystal was physically rotated about its symmetry axis during the experiment to average out any Φ_γ asymmetry in the crystal efficiency.

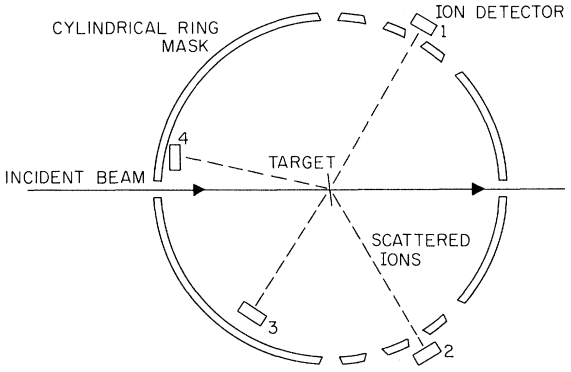

FIG. 3. Chamber arrangement for the reorientation-effect experiment.

In order to perform the experiment most efficiently and to cover a large range of ion scattering angles, ions were detected simultaneously in four ion detectors placed at different angles in the ion scattering plane. The excitation probability is extremely sensitive to scattering angle for forward scattering, so that the scattering angle must be accurately known. We have constructed a cylindrical ring with a 25-cm diam, behind which two ion detectors can be positioned symmetrically with respect to the beam axis at laboratory scattering angles of 90, 75, 60, and 45°. This cylindrical ring is aligned with respect to the scattering chamber center and incident beam direction. Using a transit, which sights along the beam line, the target is positioned with respect to the chamber center with an accuracy of ±0.3 mm. Calibration of the detectors with respect to the ion scattering angle is achieved by moving the detectors into the transit line of sight and noting the corresponding angle setting. The various circular apertures in the cylindrical ring are 1.54 cm in diameter, while the surface-barrier detectors, which are positioned behind these apertures, have a sensitive surface with a diameter of 2.39 cm. Thus, slight detector positioning uncertainties can be tolerated while retaining angle integrity. In the backward angles it is preferable to place detectors closer to the target. Inside the 26-cm cylindrical ring a third detector with its sensitive surface individually masked to a diameter of 1.9 cm is positioned at 8.25 cm from the chamber center. This detector is moved over a range from 100 to 145° in the laboratory. The fourth detector, with a sensitive surface of 2.39 cm in diameter, is fixed 7.62 cm from the chamber center at a laboratory scattering angle of 162°. The chamber arrangement is shown schematically in Fig. 3.

In order to continuously monitor the angle integrity during the reorientation experiments, the number of scattered ions in each of the four detectors is compared with the Rutherford cross section. Deviations from the Rutherford cross section are interpreted as a change in the beam position and are used to correct the data. Expressed in angular terms these corrections reflect uncertainties of <0.1°.

A simplified block diagram of the electronics is shown in Fig. 4. The data were accumulated in the form of both real and accidental gated γ spectra for each ion detector by using a random-access-time-sharing exclusive OR gate, designed by Simms,[15] to process timing signals from the ion detectors.

The linear signals from the ion detectors went

to charge-sensitive preamplifiers. The preamplified signals then went to linear amplifiers used in the double-delay-line mode, and then to integral discriminators which employed leading-edge timing. The discriminators generated a timing pulse which went to the exclusive OR gate. Cross talk between ion channels was prevented by the exclusive OR gate which placed a *common* 15-μsec dead time on all ion channels for each timing pulse accepted, allowing logic decisions to be made while letting only the initiating pulse through. The total ion-channel dead time was maintained at 6% or less by lowering beam currents when the symmetrical pair of ion detectors were located at forward scattering angles. The ion singles counting rate was obtained from the number of ion counts from a given detector which passed the exclusive OR gate. These signals were tabulated in scalers and set to the coincidence circuit.

The linear signals from large γ detector went to a charge-sensitive preamplifier, to a linear amplifier used in the double-delay-line mode, and to an integral discriminator which used leading-edge timing. The discriminator generated a timing pulse which went to a gate that gave each γ timing pulse which it processed a 10-μsec dead time in order to allow logic decisions to be made before another γ pulse was processed. The total γ-channel dead time was on the order of 2%.

The signals from the ion and γ gates went to the coincidence circuit. The coincidence circuit measured real plus accidental events, hereafter called reals, and accidental events for all ion and γ pulses with a resolving time of about $2\tau = 300$ nsec. Real and accidental coincidence pulses out of the coincidence circuit were tagged by the originating ion detector via the exclusive OR gate. Any real or accidental coincidence event opened a linear gate for the γ spectra and allowed the linear pulse which initiated the event to pass into one of the 100-channel subgroups of the analyzer. Eight γ spectra were simultaneously stored and appropriately routed as representing real and accidental events from each of the four ion detectors.

The targets were in the form of self-supporting Pd metal films ~175 μg/cm^2 thick enriched to 75.5% for Pd^{106} and 87.5% for Pd^{110}. The isotopes were obtained from the Separated Isotopes Division of the Oak Ridge National Laboratory. The targets were made by vacuum-evaporating the separated-isotope metal from Al_2O_3-coated Mo boats onto glass slides which were mounted on a substrate which was heated to 300°C. The films were floated onto water and then lifted on copper target holders which had 0.635-cm diam circular openings.

IV. TREATMENT OF DATA

The output from a reorientation-effect experiment, for a given set of ion angles, consisted of the eight gated γ spectra and the number of scattered ions in each detector which passed the exclusive OR gate. The γ spectra were processed to determine the number of real, R_i, γ rays in the photopeak coincident with ions in detector i,

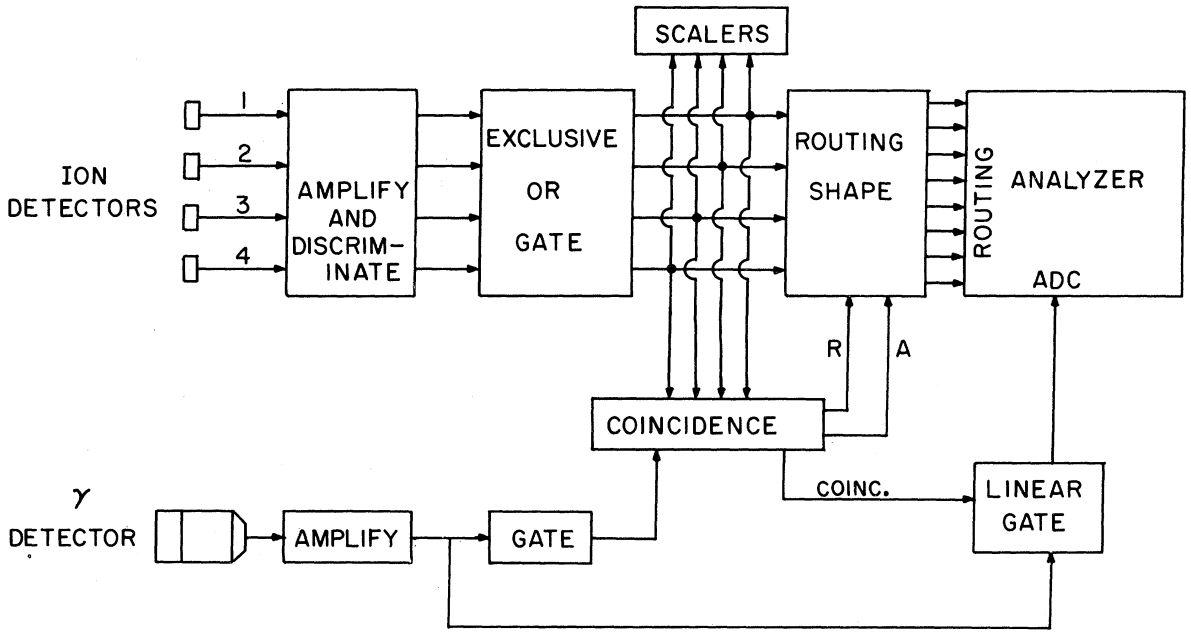

FIG. 4. Electronics diagram.

where $i = 1, 4$. The small fraction of coincidence in the photopeak due to higher-level decays was determined and subtracted. The number of ions from detector i passing the exclusive OR gate were denoted as N_i. The kinematical corrections were combined in the quantity $D_i(\theta_{\mathrm{Ion}})$.

Four measurements were made at each of four sets of scattering angles. The 162° position was repeated each time. At least 10 000 real coincidences were measured at each angle. The relative excitation probability $P_{if}(\xi, \theta_{\mathrm{Ion}})$ was obtained from

$$P_{if}(\xi, \theta_{\mathrm{Ion}}) = R_i D_i(\theta_{\mathrm{Ion}})/N_i C_i(\xi, \theta_{\mathrm{Ion}}), \quad (8)$$

where $C_i(\xi, \theta_{\mathrm{Ion}})$ is the relative crystal correction to be discussed below.

The excitation probability was parametrized as

$$P(\theta_{\mathrm{Ion}}) = A(\theta_{\mathrm{Ion}}) + M_{22} B(\theta_{\mathrm{Ion}}). \quad (9)$$

The theoretical excitation probability was calculated using M_{22} values which straddle the experimental curve, with the aid of the Winther–de Boer[16] computer program. An interpolation and least-squares fit to the experimental points was then made to obtain M_{22}.

The origin of the relative crystal correction $C_i(\xi, \theta_{\mathrm{Ion}})$ is the variation of the anisotropic particle-γ angular distribution with the ion scattering angle. Consider the focal cooridinate system of Alder *et al.*[13] shown in Fig. 5. The large γ crystal axis is situated along the z axis above the ion scattering plane. After integrating over the Φ_γ dependence, the angular distribution of the deexcitation photons seen by the large γ crystal in the focal system can be written[10]

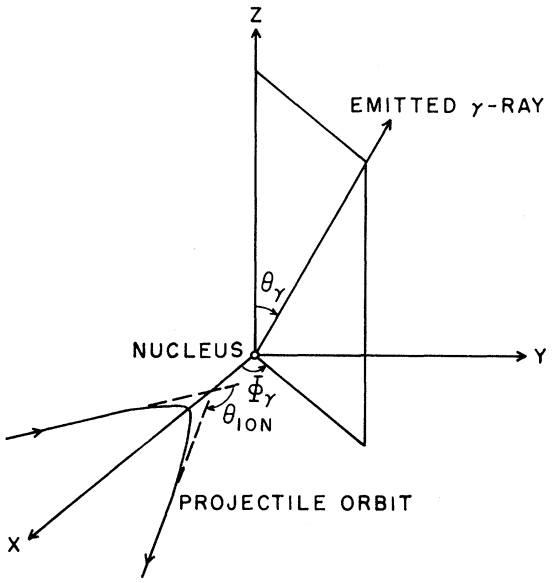

FIG. 5. Focal coordinate system.

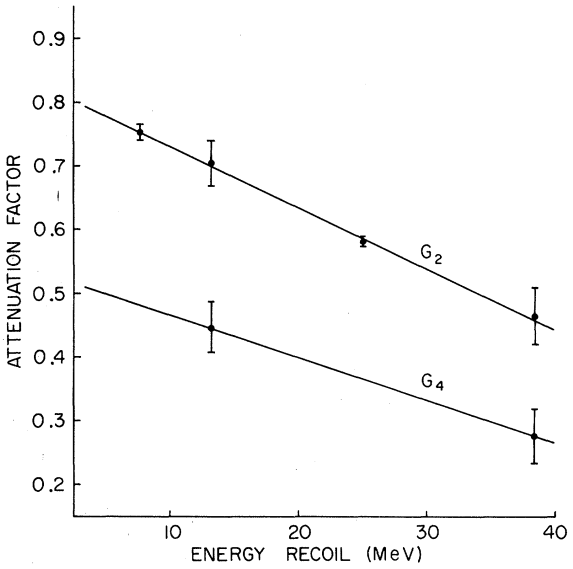

FIG. 6. γ angular distribution attenuation factor for Pd^{106}.

$$W(\theta_{\mathrm{Ion}}, \theta_\gamma, \xi) = 1 + A_2(\theta_{\mathrm{Ion}}, \xi) G_2(\theta_{\mathrm{Ion}}, \xi) P_2(\cos\theta_\gamma) + A_4(\theta_{\mathrm{Ion}}, \xi) G_4(\theta_{\mathrm{Ion}}, \xi) P_4(\cos\theta_\gamma), \quad (10)$$

where θ_{Ion} is the ion scattering angle, θ_γ is the angle of emission of the deexcitation photon with respect to the z axis, and ξ is the adiabaticity parameter. The $P_k(\cos\theta_\gamma)$ are Legendre polynomials, and the $A_k(\theta_{\mathrm{Ion}}, \xi)$ are proportional to the statistical tensors for the distribution. The $G_k(\theta_{\mathrm{Ion}}, \xi)$ are the attenuation coefficients.

If the excited target nucleus recoils out of the target before decay occurs, the nucleus can be subject to large electric and/or magnetic fields at

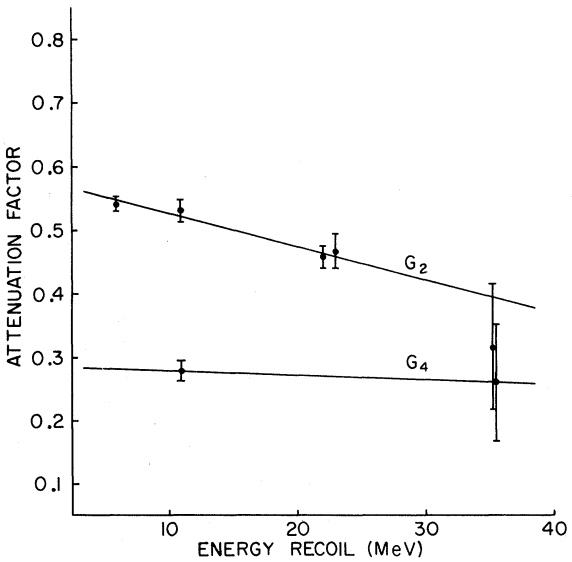

FIG. 7. γ angular distribution attenuation factor for Pd^{110}

the nucleus due to ionization of the atomic electron cloud. These fields can interact with the nuclear moments and cause precession of the angular momentum vector of the excited nuclear state before decay. Since the degree of ionization of the atomic electron cloud can depend on the recoil energy, the amount of precession can depend on the incident-ion scattering angle. The precession results in attenuation of the γ angular distribution as manifested in the attenuation coefficients $G_k(\theta_{\mathrm{Ion}}, \xi)$.

The crystal correction $C_i(\xi, \theta_{\mathrm{Ion}})$ compensates for the anisotropic photon angular distribution. The number of γ coincidence counts in the large γ crystal was modified by the crystal correction so that the modified γ counts represented an equal opportunity for any inelastic ion which was detected of having its associated deexcitation photon observed by the large γ crystal. The attenuation factors $G_k(\theta_{\mathrm{Ion}}, \xi)$ in Eq. (10) were obtained by observing the angular distribution of the deexcitation γ photons in the ion scattering using a small 3.82-cm $\times$2.54-cm NaI(Tl) crystal. The total γ distribution and a distribution coincident with backscatter ions observed in an annular ion detector were taken. If the perturbing force causing the attenuation is randomly oriented, the attenuation coefficients relevant to the γ distributions in the ion scattering

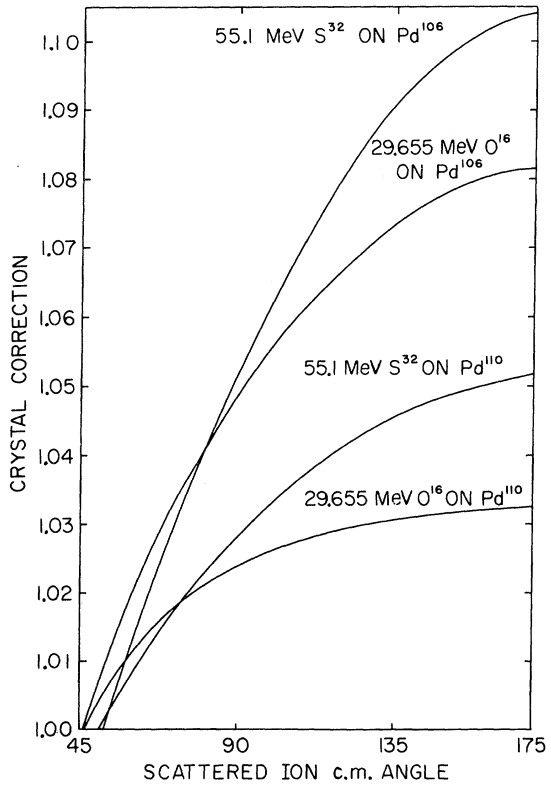

FIG. 8. Relative crystal correction for 9-in. $\times$ 4-in. NaI(Tl) crystal.

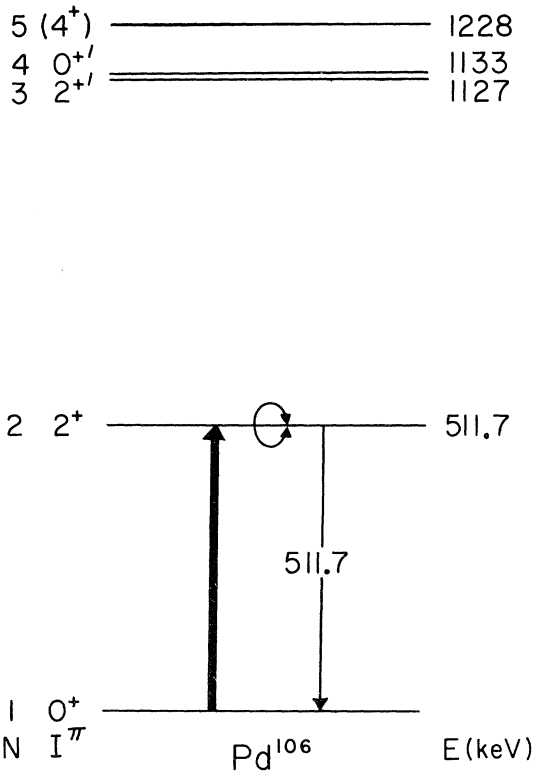

FIG. 9. Energy level diagram for low-lying states of Pd^{106}.

plane are identical to the attenuation coefficients in the distribution seen by the large γ crystal and shown in Eq. (10).[17] The experimentally determined attenuation factors for Pd^{106} and Pd^{110} are shown in Figs. 6 and 7.

The relative γ detector angular efficiency $\epsilon(\theta_\gamma)$ was measured with a collimated γ-ray source for several γ-ray energies. An accurate interpolation

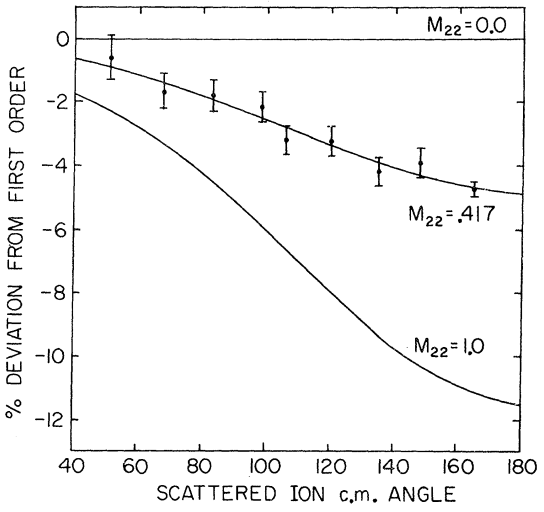

FIG. 10. Summary of 30-MeV O^{16} on Pd^{106} experiments.

to the exact γ-ray energy could be made since the angular dependence of the efficiency was insensitive to the precise energy. No Φ_γ asymmetry was detected.

The relative crystal correction $C_i(\xi, \theta_{\mathrm{Ion}})$ was computed by numerically integrating the experimentally determined photopeak efficiency $\epsilon(\theta_\gamma)$ and the ion-γ directional correlation $W(\theta_{\mathrm{Ion}}, \theta_\gamma, \xi)$ (obtained from the Winther-de Boer program), over the large γ crystal. The ion-γ correlation is insensitive to M_{22}, and, consequently, the crystal correction is essentially independent of M_{22}.[18] The relative crystal correction is shown in Fig. 8.

V. RESULTS

The energy levels[19] for the low-lying states in Pd^{106} are shown in Fig. 9. Both the one-phonon 2^+ state and the two-phonon 0^+, 2^+, 4^+ triplet states are present, indicating Pd^{106} has an energy spectrum characteristic of a pure vibrational nucleus. Summary plots of the reorientation-effect results are shown in the form of percentage deviations from first-order theory as a function of ion scattering angle in Figs. 10 and 11. The percentage deviation from first order is defined by

$$(P_{02}^{(12)}/P_{02}^{(11)}) \times 100. \quad (11)$$

The energy levels[19] for the low-lying states in Pd^{110} are shown in Fig. 12. In addition to the one-phonon 2^+ state and the two-phonon 0^+, 2^+, 4^+ triplet states, Pd^{110} also has a third 2^+ state at 1212 keV. The spectrum of Pd^{110} is characteristic of a pure vibrational nucleus although the third 2^+ state indicates some deviation from the pure vibrational model. The reorientation-effect experiments were performed by scattering 25- and 30-MeV O^{16}, and 55- and 56-MeV S^{32} ions off Pd^{110} nuclei. Summary plots of the results are shown in the form of percentage deviations from first-order theory as a function of ion scattering angle in Figs. 13–16.

In order to avoid complications due to the nuclear force and to justify the assumption that the interaction is purely electromagnetic, a substantial physical separation must be maintained between target and projectile ion. In these experiments the nuclear surfaces of projectile and target were separated by at least 10 F.

Douglas and McDonald[20] have shown that the excitation of the first 2^+ state via the giant-dipole-resonance interference is considerably smaller than the reorientation effect. In addition, for different projectiles, whose incident energies are chosen so that the values of the adiabaticity parameter ξ are the same, the relative magnitudes of

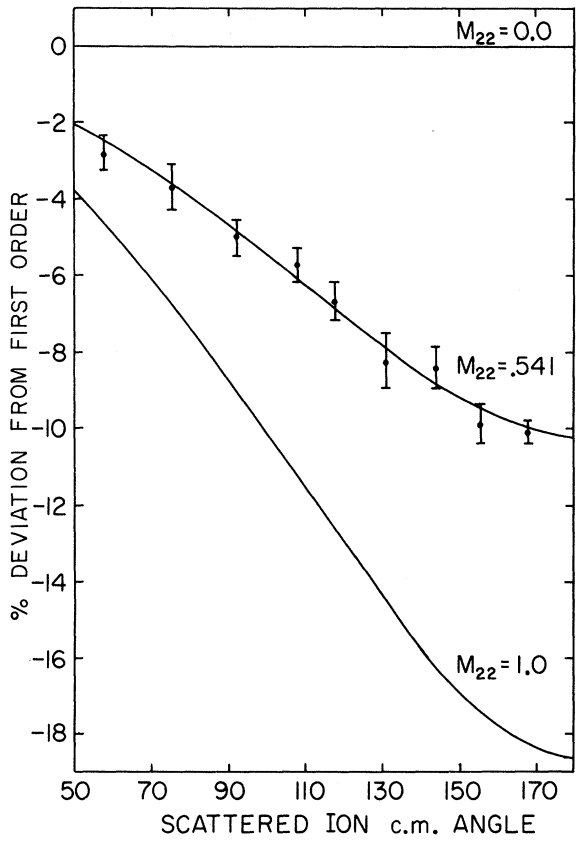

FIG. 11. Summary of 56-MeV S^{32} on Pd^{106} experiments.

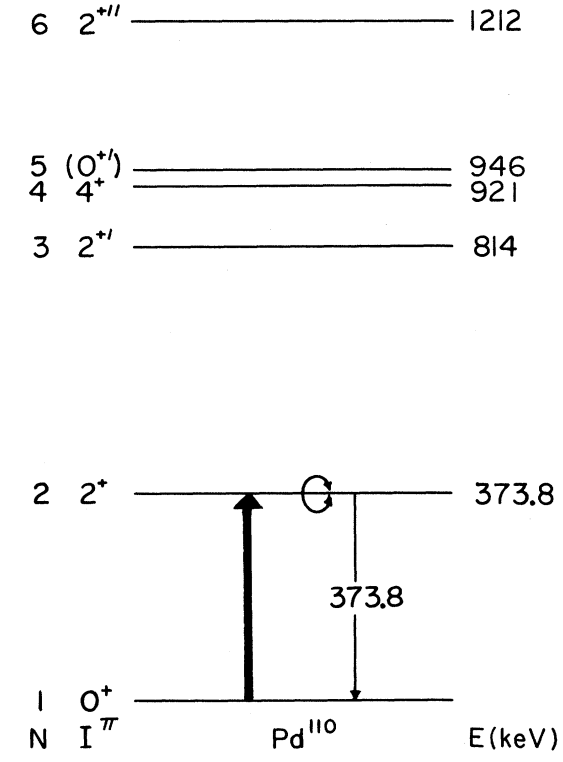

FIG. 12. Energy-level diagram for low-lying states of Pd^{110}.

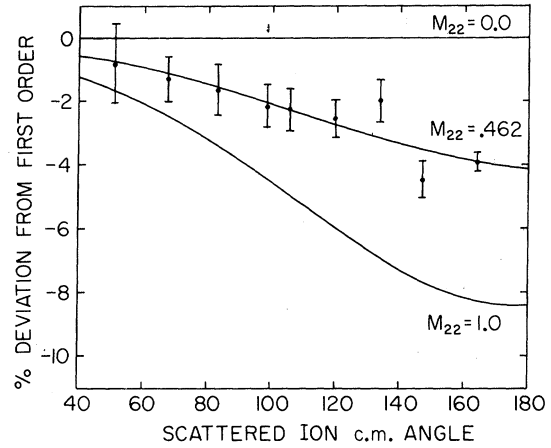

FIG. 13. Summary of 25-MeV O^{16} on Pd^{110} experiments.

the interference via the giant-dipole and the reorientation effect remain constant. Therefore, consistency of the oxygen and sulfur results should be completely independent of the giant-dipole interference term. Comparison of the oxygen and sulfur results thus can be used to indicate the sign of the interference via the second 2^+ state.

In Figs. 17 and 18 the percentage change in the excitation probability due to the interference term from excitation via the second 2^+ state is shown for Pd^{106} and Pd^{110}. The interference must be considered for the energies at which the experiments were performed. For notational purposes the sign of the matrix-element product relevant to the second 2^+ state interference will be indicated by $\mathcal{P}_4$, where

$$\mathcal{P}_4 = |M_{12}M_{23}M_{13}M_{22}|/M_{12}M_{23}M_{13}M_{22}. \quad (12)$$

$\mathcal{P}_4$ is independent of the phase convention chosen for the matrix elements. For $\mathcal{P}_4 < 0$ the interference due to the second 2^+ state is positive,

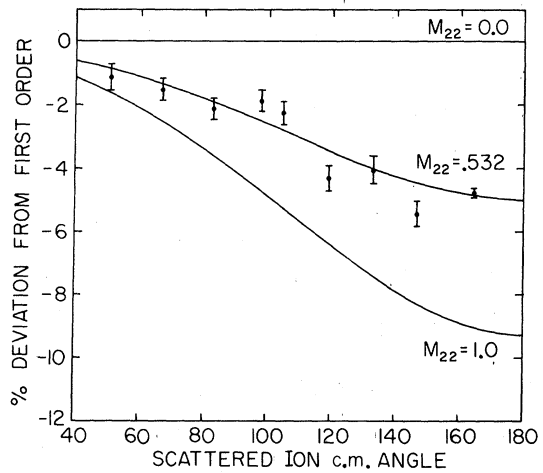

FIG. 14. Summary of 30-MeV O^{16} on Pd^{110} experiments.

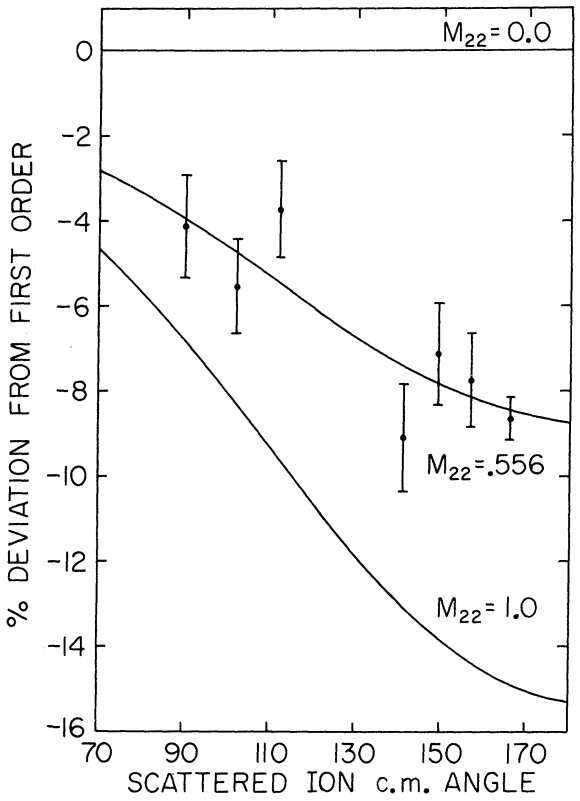

FIG. 15. Summary of 55-MeV S^{32} on Pd^{110} experiments.

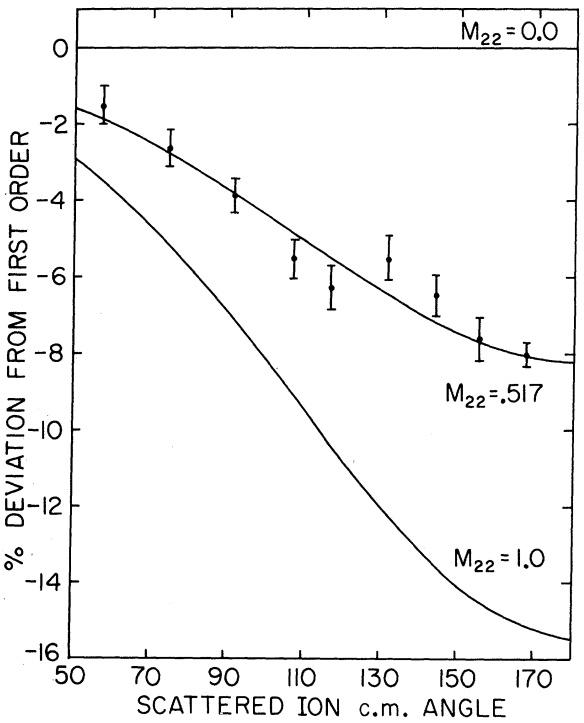

FIG. 16. Summary of 56-MeV S^{32} on Pd^{110} experiments.

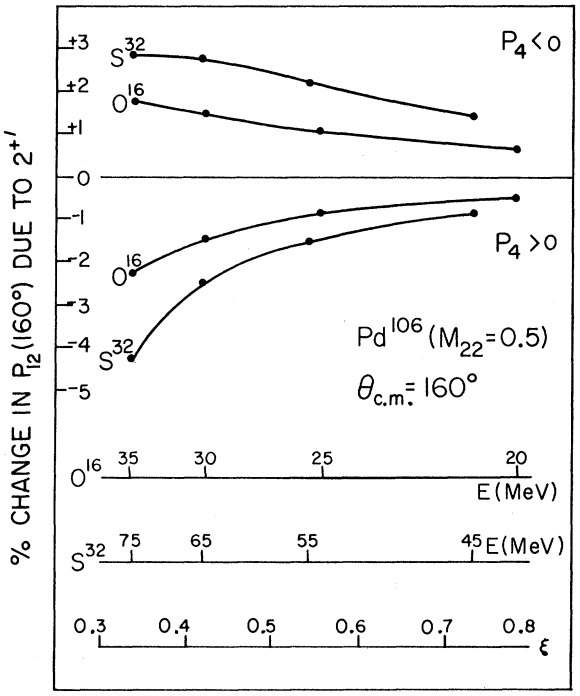

FIG. 17 Percentage change in excitation probability of first excited 2^+ state due to interference from excitation via the second excited 2^+ state for Pd^{106}.

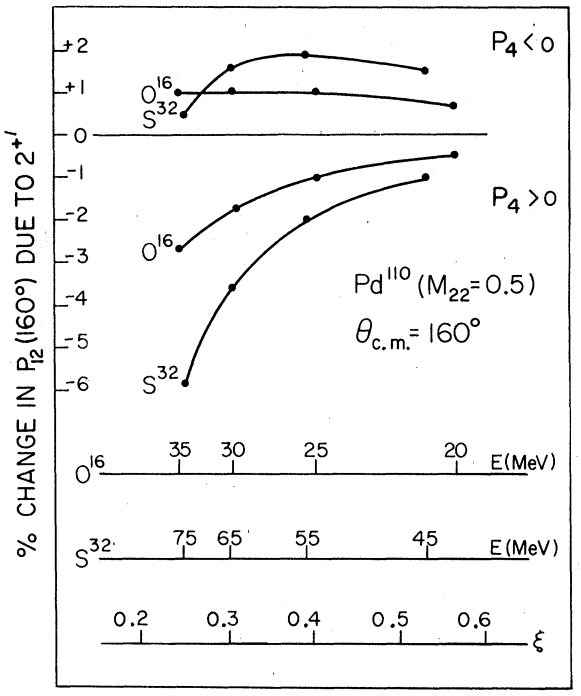

FIG. 18. Percentage change in excitation probability of first excited 2^+ state due to interference from excitation via the second excited 2^+ state for Pd^{110}.

increasing the excitation probability of the first 2^+ state. For $\mathcal{P}_4 > 0$ the interference due to the second 2^+ state is negative, decreasing the excitation probability of the first 2^+ state.

In Table I the results extracted from the data are displayed. In the column headed M_{22}(2 level) the M_{22} values obtained by considering the nuclei to have only two energy levels (ground state and first excited 2^+ state) are listed. In the columns headed $M_{22}(\mathcal{P}_4 < 0)$ and $M_{22}(\mathcal{P}_4 > 0)$, the M_{22} values obtained by considering the nuclei to have three energy levels (ground state, first and second excited 2^+ states) are listed for each sign of the second excited 2^+ state interference term. The uncertainty in the M_{22} values is listed in the column headed error. A third 2^+ state ($N = 6$) in Pd^{110} was not considered in this calculation, because of its small coupling to the first 2^+ state. For Pd^{106} the oxygen and sulfur results are more consistent for positive interference, $\mathcal{P}_4 < 0$, than for negative interference, $\mathcal{P}_4 > 0$. Therefore, if we use self-consistency of the oxygen and sulfur results as a criteria, the interference from the second 2^+ state on the excitation of the first 2^+ state appears to be

TABLE I. Results.

Target	Beam	Energies (MeV)	M_{22}(2 Level)	$M_{22}(\mathcal{P}_4 < 0)$	$M_{22}(\mathcal{P}_4 > 0)$	Error
Pd^{106}	O^{16}	30	0.417	0.546	0.283	0.113
	S^{32}	56	0.541	0.659	0.458	0.109
	Average		0.481	0.604	0.370	0.078
		$Q_{22} = -0.458 \pm 0.059$ b	$(\mathcal{P}_4 < 0)$			
		$Q_{22} = -0.282 \pm 0.059$ b	$(\mathcal{P}_4 > 0)$			
Pd^{110}	O^{16}	25–30	0.503	0.617	0.318	0.087
	S^{32}	55–56	0.531	0.657	0.389	0.097
	Average		0.516	0.637	0.350	0.065
		$Q_{22} = -0.483 \pm 0.049$ b	$(\mathcal{P}_4 < 0)$			
		$Q_{22} = -0.266 \pm 0.049$ b	$(\mathcal{P}_4 > 0)$			

positive ($\mathcal{P}_4 < 0$). If the experiments are considered individually then two values of the quadrupole moment can be extracted from the data. An independent measurement of $\mathcal{P}_4$ could settle this question.

VI. COMMENTS

The excitation-probability curves, Figs. 10, 11, 13–16, indicate deviations from first-order theory that are consistent with nonzero static quadrupole moments. These substantial moments are in disagreement with the zero moments predicted by the pure vibrational model of the nucleus.

Tamura and Udagawa[11] have introduced a phenomenological anharmonic-vibrator model of the nucleus. They consider the wave functions of the first and second excited 2^+ states to be

$$\Psi_{2^{+\prime}} = (1-\alpha^2)^{1/2} |2^{+\prime}\rangle - \alpha |2^+\rangle , \tag{13}$$

$$\Psi_{2^+} = \alpha |2^{+\prime}\rangle + (1-\alpha^2)^{1/2} |2^+\rangle , \tag{14}$$

where $|2^+\rangle$ and $|2^{+\prime}\rangle$ are the pure one- and two-quadrupole phonon states. In this model the static and transition quadrupole moments of the first and second excited 2^+ states and the ground state can be expressed in terms of the mixing parameter $|\alpha|$. In particular,

$$Q_{22} = \tfrac{12}{5}(7\pi)^{-1/2}\alpha(1-\alpha^2)^{1/2} Z R_0^2 \beta \tag{15}$$

is expressed in terms of α, R_0, and β, the amplitude of the quadrupole-type surface vibration. With this model substantial quadrupole moments occur if the 2^+ state contains large mixtures of the one- and two-phonon excitations.

Further, the anharmonic-vibrator model relates the sign of the interference in the excitation probability of the first excited 2^+ state due to excitation via the second excited 2^+ state with the sign of the static quadrupole moment of the first 2^+ state.[21,22] This model predicts a positive interference term for a negative static quadrupole moment. This agrees with the self-consistent interpretation of these Pd^{106} experiments and the conclusions of Cline[22] in reanalyzing the available data on the static quadrupole moment of the first excited 2^+ state in Cd^{114}.

However, Robinson *et al.*[19] have shown that no single admixture can explain the ratio of matrix elements,

$$\frac{B(E2, 2^{+\prime} \to 2^+)}{B(E2, 2^+ \to 0^+)}, \quad \frac{B(E2, 2^{+\prime} \to 0^+)}{B(E2, 2^+ \to 0^+)}, \tag{16}$$

in these palladium isotopes.

In Table II the values of the admixture parameter $|\alpha|$ necessary to account for the static quadrupole moments from this experiment are listed along with the values of the admixture parameter necessary to account for the ratio of the transition moments as determined by Robinson *et al.*[19] No single admixture can explain the transition moment ratios and static quadrupole moments. The lack of agreement between the amounts of admixture necessary to explain the experimental moments argues against a simple representation in terms of vibrational quadrupole phonons.

Baranger and Kumar[23] have solved Bohr's collective Hamiltonian numerically using a pairing-plus-quadrupole model. They are able to account for vibrational-type spectra, as well as substantial static quadrupole moments for the first 2^+ excited state through a coupling of rotational and vibrational motions yielding a nonzero equilibrium deformation. While no explicit pairing-plus-quadrupole-model calculations are presently available in this mass region, the model predicts the sign of $\mathcal{P}_4$ in terms of the character of the second 2^+ state. If the second 2^+ state is interpreted as a 2^+_γ vibration, then $\mathcal{P}_4 < 0$. If the second 2^+ state is interpreted as a 2^+_β vibration, then $\mathcal{P}_4 > 0$. The observed energy spectrum suggests the 2^+_γ assignment.

The static quadrupole moments predicted by the pure rotational model of the nucleus are

$$Q_{22}(\text{rot}) \simeq 0.75 \text{ b for } Pd^{106},$$
$$Q_{22}(\text{rot}) \simeq 0.85 \text{ b for } Pd^{110}. \tag{17}$$

The absolute value of the static quadrupole moments obtained in this experiment therefore is considerably smaller than the pure rotational model predicts and larger than the pure vibrational model predicts. This indicates that the first excited 2^+ states in the Pd isotopes may represent a motion that is "intermediate" to that of the

TABLE II. Anharmonic-vibrator-model admixtures. Values of $|\alpha|$ necessary to explain experimentally determined moments.

	$\frac{B(E2, 2^{+\prime} \to 2^+)}{B(E2, 2^+ \to 0)}$	$\frac{B(E2, 2^{+\prime} \to 0^+)}{B(E2, 2^+ \to 0)}$	Q_{22}(expt) ($\mathcal{P}_4 < 0$)	Q_{22}(expt) ($\mathcal{P}_4 > 0$)
Pd^{106}	0.435	0.16	0.30	0.18
Pd^{110}	0.428	0.118	0.26	0.14

strongly deformed rotational and pure vibrational-type motions.

ACKNOWLEDGMENTS

The authors are indebted to the staffs of the Purdue University and Argonne National Laboratory tandem acceletators. They are indebted to Professor R. M. Steffen for his interest and support, and to Professor P. C. Simms for his aid in designing the electronics. The aid of W. Lutz and P. Sioshansi in accelerator operation is gratefully acknowledged.

---

*Work supported by the U. S. Atomic Energy Commission under Contract No. AT(11-1)1746 (Chicago Operations Office).

†Present address: Department of Physics, Wittenberg University, Springfield, Ohio 45501.

[1]A. Bohr, Kgl. Danske Videnskab. Selskab, Mat.-Fys. Medd. 26, No. 14 (1952).

[2]A. Bohr and B. R. Mottelson, Kgl. Danske Videnskab. Selskab, Mat.-Fys. Medd. 27, No. 16 (1963).

[3]J. de Boer, R. Stokstad, G. Symons, and A. Winther, Technical Report, California Institute of Technology, 1965 (unpublished).

[4]R. G. Stokstad, I. Hall, G. D. Symons, and J. de Boer, Nucl. Phys. A92, 319 (1967).

[5]J. J. Simpson, D. Eccleshall, M. J. L. Yates, and N. J. Freeman, Nucl. Phys. A94, 177 (1967).

[6]P. H. Stelson, W. T. Milner, J. L. C. Ford, Jr., F. K. McGowan, and R. L. Robinson, Bull. Am. Phys. Soc. 10, 427 (1965).

[7]P. H. Stelson, in Proceedings of the Summer Group on the Physics of the Emperior Tandem Van de Graaff Region, Brookhaven National Laboratory, 1965 (unpublished), Vol. III, p. 1005.

[8]J. E. Glenn and J. X. Saladin, Phys. Rev. Letters 19, 33 (1967).

[9]G. Schilling, R. P. Scharenberg, and J. W. Tippie, Phys. Rev. Letters 19, 318 (1967).

[10]G. Schilling, R. P. Scharenberg, and J. W. Tippie, Phys. Rev. C 1, 1400 (1970).

[11]T. Tamura and T. Udagawa, Phys. Rev. 150, 783 (1966).

[12]G. Breit and J. P. Lazarus, Phys. Rev. 100, 942 (1955); G. Breit, R. Gluckstern, and J. E. Russell, Phys. Rev. 103, 727 (1956); G. Breit and R. L. Gluckstern, in *Handbuch der Physik*, edited by S. Flügge (Springer-Verlag, Berlin, Germany, 1959), Vol. XLI, p. 496.

[13]K. Alder, A. Bohr, T. Huus, B. Mottelson, and A. Winther, Rev. Mod. Phys. 28, 432 (1956).

[14]J. de Boer and J. Eichler, in *Advances in Nuclear Physics*, edited by M. Baranger and E. Vogt (Plenum Press, New York, 1968), Vol. I.

[15]P. C. Simms, private communication.

[16]A. Winther and J. de Boer, A Computer Program for Multiple Coulomb Excitation, Progress Report, Rutgers, The State University, and California Institute of Technology, 1965 (unpublished).

[17]R. M. Steffen, private communication.

[18]G. Schilling, M.S. thesis, Case Institute of Technology, 1963 (unpublished).

[19]R. L. Robinson, F. K. McGowan, P. H. Stelson, W. T. Milner, and R. O. Sayer, Nucl. Phys. A124, 553 (1969).

[20]A. C. Douglas and N. McDonald, Phys. Letters 24B, 447 (1967).

[21]T. Tamura, Phys. Letters 28B, 90 (1968).

[22]D. Cline, Bull. Am. Phys. Soc. 14, 726 (1969).

[23]M. Baranger and K. Kumar, Nucl. Phys. 62, 113 (1965); A110, 490 (1968); A122, 241 (1968); K. Kumar and M. Baranger, Nucl. Phys. A110, 529 (1968); A122, 273 (1968); Phys. Rev. Letters 17, 1146 (1966).